

# Numerical–experimental investigations on the manufacturing of an aluminium bipolar plate for proton exchange membrane fuel cells by warm hydroforming

G. Palumbo · A. Piccininni

Received: 12 October 2012 / Accepted: 29 April 2013 / Published online: 25 May 2013  
© Springer-Verlag London 2013

**Abstract** This research study focuses on the manufacturing of a bipolar plate used in proton exchange membrane fuel cells. In particular, the authors investigate the manufacturing of the part by means of warm hydroforming, adopting an aluminium alloy (AA6061) as sheet material. Both the channel profile (the reagent channel width and the die upper radius), and the bipolar plate geometries (in terms of channel layouts) are investigated by means of finite element simulations. Preliminary experimental investigations were carried out in order to define both the mechanical (flow curves) and strain behaviours (forming limit curves) of the adopted aluminium alloy according to temperature and strain rate. Subsequent finite element investigations aimed to define the channel profile by means of 2D models: a statistical approach was used to evaluate the dimension of the reagent channel width, the die upper radius and the sheet thickness. Finally, proposed bipolar plate geometries were investigated by running 3D simulations at different working temperatures and oil pressures in order to evaluate: (1) the bipolar plate geometry able to avoid regions with critical thinning and (2) suitable parameters for the warm hydroforming process.

**Keywords** Warm hydroforming · Bipolar plate · Aluminium alloys · Finite element

## 1 Introduction

Fuel cells (FCs) can directly convert the chemical energy of fuels into electrical energy, providing high levels of efficiency and low environmental impact. Among different types of FCs, the proton exchange membrane FC (PEMFC) represents one of the most attractive alternatives to conventional internal combustion engines due to its great number of advantages: (1) minimum noise level during working, (2) compact size, (3) high power density, (4) low working temperature and (5) almost zero hazardous emissions [1]. Figure 1 shows the main components of a PEMFC: the ion exchange membrane, the electro-catalyst at the interface between the backing layer and the membrane and the bipolar plate (BP), or flow plate, which delivers fuel and oxidant to reactive sites.

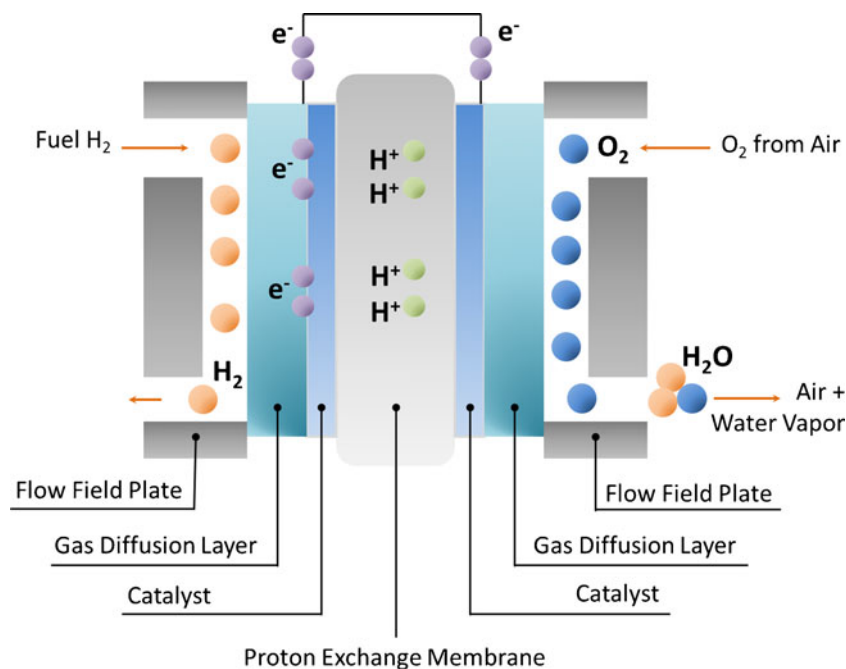
The BP plays a strategic structural and functional role in the PEMFC; in fact, this component (the most important as regards the total weight of the device since it represents about 75 % of the PEMFC's mass) performs a number of fundamental functions, such as (a) carrying fuel and air to the corresponding electrodes, (b) conducting electric current through the FC and (c) providing mechanical support for the entire stack. For the majority of PEMFC applications, single FCs are combined in a modular way in order to obtain a stack: one of the most commonly used arrangements is the so-called *planar bipolar arrangement* [1].

With this concept in mind, in order to make the PEMFC a feasible energy system for applications not only in fixed installations but also in transport (mostly automotive) and electronic fields (laptops for example), possible solutions could be: (1) to improve the efficiency of the PEMFC, (2) to

---

G. Palumbo (✉) · A. Piccininni  
Department of Mechanical Engineering, Mathematics &  
Management Engineering, Politecnico di Bari,  
Viale Japigia 182,  
Bari, Italy  
e-mail: g.palumbo@poliba.it

**Fig. 1** General diagram of PEMFC



increase the energy density of the PEMFC and (3) to reduce the weight of the BP.

As far as the first solution is concerned (efficiency improvement), studies were carried out in order to evaluate optimal working conditions (pressure and reagent flow rate) which are able to maximise FC efficiency, according to specific BPs designs [2]. The second solution (energy density increase) could be obtained by minimising the thickness of the BP [3]. The implementation of the third solution (weight reduction) requires the adoption of materials able to guarantee not only good mechanical characteristics, optimal electrical conductivity and impermeability to gas but also high corrosion resistance and low surface electrical resistance. The first types of BPs were fabricated from graphite and carbon composites because of their low contact resistance and relatively high corrosion resistance. However, graphite and carbon composites, despite showing good performance in an FC-operating environment, cannot be considered as the best choice since they are brittle, bad electrical and thermal conductors, gas permeable and rather costly to be machined [4]. This explains why metals are considered a more attractive alternative for the production of BPs [5].

Several research studies have been carried out with the aim of studying the performance of sheet metals for the production of a BP. Attention has focused mainly on stainless steel and aluminium (Al) alloys. Stainless steel, although characterised by good mechanical strength and machinability, provides limited contact resistance [6], resulting in a low power density and high power losses. In order to overcome such limitations, Turan et al. [7] investigated the adoption of the hydroforming (HF) process instead of the standard stamping process. They found that the HF

process allows for the production of a BP characterised by a lower level of interfacial contact resistance (ICR) than stamping. In addition, increasing clamping load or maximum oil pressure leads to a reduction of the ICR value. Al alloys can meet the requirements of mass reduction better than stainless steel (Al density,  $2.70 \text{ g/cm}^3$ ). In addition, sheet metal processes can be used for manufacturing Al parts, thus leading to both a dramatic reduction in thickness (and consequently an increase in energy density) and optimal characteristics (excellent surface finish and good mechanical properties). It is worth noting that both stainless steel and Al alloys become rapidly corroded in a typical FC environment: investigations on the effect of ZrN coating on SS316L sheets [8] revealed that higher corrosion resistance could be obtained but with a lower level of formability and lower values of ICR. Experiments conducted on AA5083 specimens coated with CrN obtained lower ICR values than the uncoated ones, while no appreciable variation in ICR was detected for different values of the coating thickness [9].

In addition to the question of corrosion, if Al alloys are used in the production of BPs, the most important problem to be addressed is the poor formability of these materials, which is much more limited than deep drawing steels. However, as confirmed by literature, this restriction can be overcome by performing the process in warm conditions (temperatures much lower than  $350 \text{ }^\circ\text{C}$ ) and using proper strain rates [10–13]. In particular, since previous investigations have confirmed the feasibility of using the HF technique for manufacturing complex-shaped parts [14, 15] and in particular the channels of a BP [7, 16, 17], in this study the HF in warm conditions (WHF) is proposed for the manufacture of an Al alloy BP. The aim of this research was to

determine, through a numerical approach, both the channel profile (the reagent channel width and the die upper radius) and the BP geometry (in terms of channel layouts) able to avoid regions with critical thinning. Furthermore, 3D FE simulations were run in order to evaluate the process parameters for the manufacturing of the BP by WHF when adopting a moderate temperature increase (up to 220 °C), with the aim of improving the characteristics of the formed part but avoiding an overly long and complex manufacturing process.

## 2 Investigated BP geometries

Since a sheet metal forming process was considered in this study rather than a machining process, the geometries of the BP (i.e. the channel layout) were designed in order to allow for (1) the manufacturing of channels on both sides in a single forming step and (2) the separation of the reagents and the coolant. Table 1 shows the three die geometries investigated in this study, labelled as *serpentine* (SER), *spiral* (SP) and *multiple serpentine* (MSER).

Stacked cells can be obtained using identical BPs with the proposed geometries as shown in the assemblies in Fig. 2

The following features are worth noting:

1. For BP-type SER and MSER, a single PEMFC unit is created assembling two BPs rotated by 90°, while cells created using the BP-type SP are characterised by two consecutive BPs with the same orientation (this simplifies the automated assembly of the cell, and eventually allows us to combine the forming process with the joining one [14]).
2. For BP-type SER and MSER, reactant gases and cooling water can be supplied from the side, while in BP-type SP the reactants have to be supplied through holes, which can be manufactured after or during the HF process. In order to reduce the component cycle time and, as a consequence, the total production cost, the HF process can be successfully integrated with subsequent operations, such as piercing [18].

## 3 Material and properties

The numerical analyses carried out in this work were performed considering the alloy AA6061-T6 as the sheet material for the BP. A preliminary experimental step aimed at characterising both the mechanical and deformative behaviour of the alloy was thus performed using sheets with a thickness of 0.5 mm.

### 3.1 Mechanical characterisation

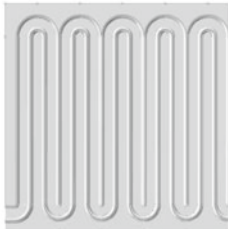
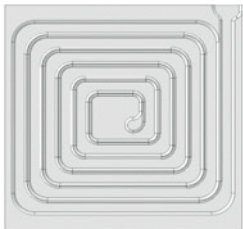

#### 3.1.1 Equipment

Tensile tests were carried out in order to evaluate material behaviour according to temperature and strain rate. Dog-bone specimens with a gauge length of 100 mm and a width of 15 mm were cut by laser beam. The equipment used for tensile tests is shown in Fig. 3: it consists of a heating device which was assembled on a 20-ton electromechanical INSTRON machine. The device, designed specifically for this experiment, was characterised by nine radiant heaters positioned around the specimen. Each group, made up of three heaters, was managed by one of the arms of the PID controller in order to reach and maintain the target temperature ( $\pm 1\%$ ); this control was based on the data collected during the process by a thermocouple in contact with the specimen. The equipment allowed us to monitor the entire test using two cameras (1.3 Mp sensors) from the Digital Image Correlation (DIC) system ARAMIS. Indeed, since images are discretised in a cell grid and automatically recognised by the system, it was possible to calculate displacements and strains continuously during the process without the need for any contact with the specimen.

#### 3.1.2 Tests and results

Tests were carried out at three temperature ( $T$ ) levels: room temperature (RT), 110 and 220 °C; two different strain rate (SR) levels were set, 0.013 and 0.0013 s<sup>-1</sup>. At each level of  $T$  and SR, specimens cut in the rolling direction were used. A set of images for a number of tested specimens acquired

**Table 1** Die geometries investigated in this work

Geometry	Serpentine	Spiral	Multiple Serpentine
Abbreviations	SER	SP	MSER
Plant view			

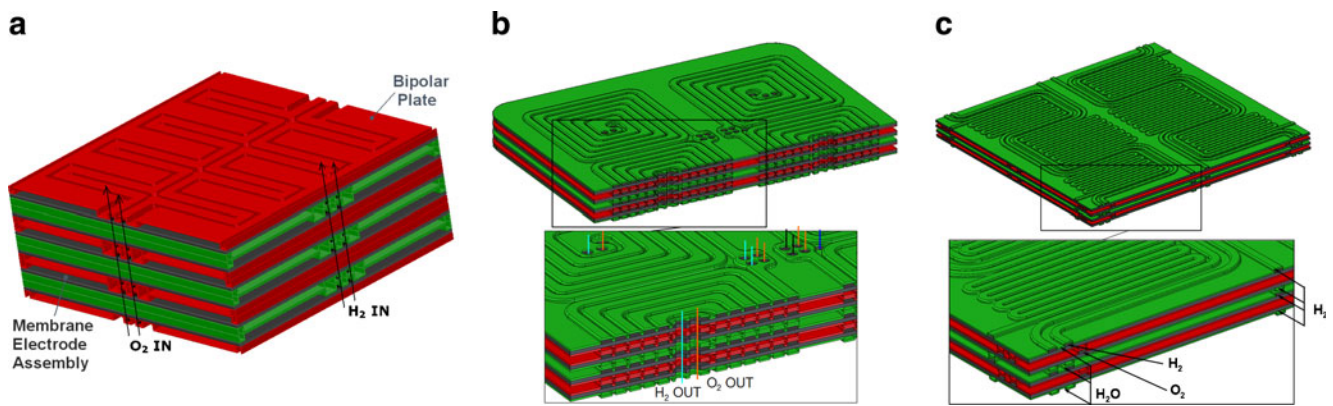


**Fig. 2** BPs assembled to create a stack: **a** SER, **b** SP and **c** MSER

by the DIC system (with corresponding maps of major strain superimposed on the deformed shape) are shown in Fig. 4, while in Fig. 5 the flow stress curves (in terms of real stress and real strain) are plotted.

It can be seen that, irrespective of the moderate temperature increase, the reduction of the flow stress is significant. Similar results were obtained by Mahabunphachai and Koç [19] in their experimental activity carried out on the same alloy but up to a higher temperature (300 °C). Moreover, although the SR effect is evident from the graph in Fig. 5, it is relatively low (as also confirmed in the work of Johansson et al. [20]), if compared with other Al alloys (for example, the 5xxx alloy) which exhibit higher ductility and a more pronounced effect of temperature on deformative behaviour. According to the study carried out by Mahabunphachai and Koç [19], better results could be obtained if the temperature is increased up to 300 °C but principally in terms of flow stress reduction (with a small difference in elongation also at higher temperature). Thus, in the present study, the authors decided to focus attention on moderate temperature increase (up to 220 °C).

### 3.2 Formability evaluation

The formability was evaluated by measuring the maximum strains the material could experience in a plane stress state in both the principal directions (major and minor strains) when subjected to various strain states, as determined by Nakazima tests. Tests were carried out at different temperature levels (the same as in the tensile tests), and the forming limit curve (FLC) was obtained for each temperature. The standard ISO 12004-2: 2008 was adopted for the FLC valuation [21].

#### 3.2.1 Equipment

The Nakazima tests were carried out using specific equipment assembled on the tensile test machine. This consisted

of a hemispherical punch (diameter 90 mm) heated by two electrical band heaters (750 W each), a circular draw die (diameter 105 mm) and a blankholder ring with a draw bead at a radial position of 140 mm. In addition, two DIC system sensors were embedded in the equipment in order to acquire a complete strain field during the deformation of the blank by the Nakazima punch.

The temperature of the specimen was monitored by means of both a thermocouple placed on the bottom surface and a pyrometer acquiring values on the upper surface. High Temperature Grease (a Teflon-based lubricant supplied by Interflon), composed of a mixture of synthetic oil, inorganic thickener, Teflon® and additives, was used since it was suitable for the range of −25 to +260 °C. In addition, in order to prevent material drawing, a blank holder force equal to 20 kN was adopted. As suggested by the ISO 12004-2 standard, the geometry of the specimens was characterised by the same length but with different widths. The standard [21] suggests a minimum number of 5 geometries for a complete FLC description; in order to limit experiment costs mainly due to the difficulties when

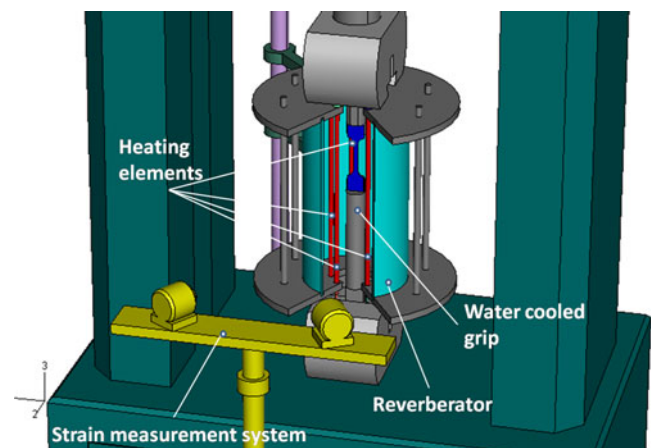


**Fig. 3** Experimental equipment for tensile tests assisted by the DIC system



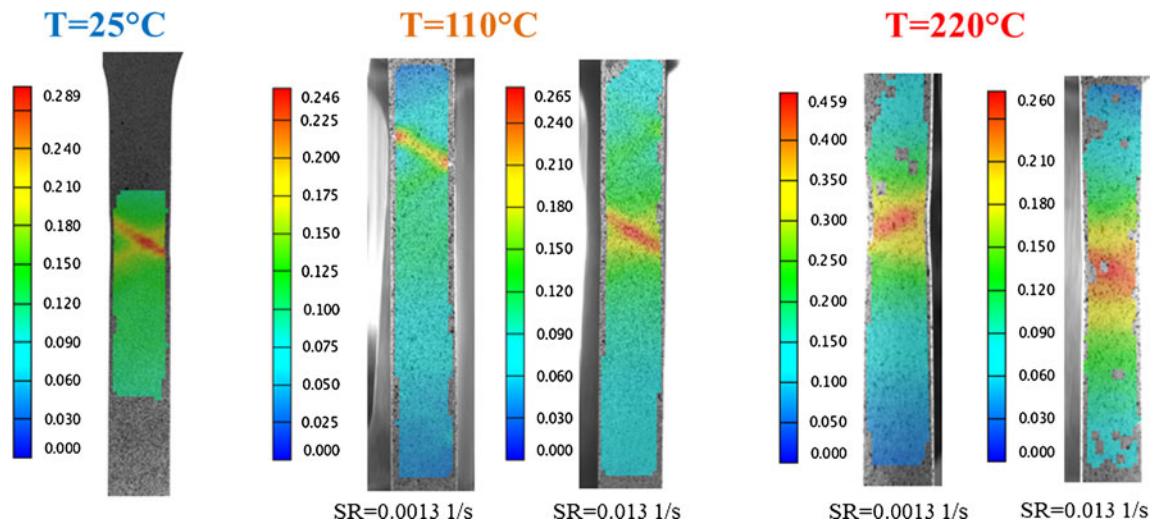
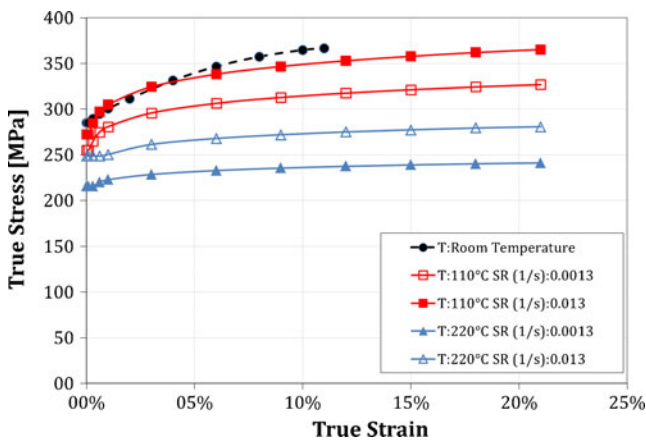


**Fig. 4** Major strain maps superimposed on the deformed shape of specimens used for mechanical characterisation by means of tensile tests at different temperatures and strain rates

working in warm conditions, only four geometries were used for the Nakazima test: width, 25 mm; width, 75 mm; width, 125 mm and width, 175 mm. Additional information deriving from the tensile test was used to evaluate the FLCs.

### 3.2.2 Tests and results

Tests were carried out at RT,  $T=110\text{ }^{\circ}\text{C}$  and  $T=220\text{ }^{\circ}\text{C}$ . The punch speed was kept constant in all tests (30 mm/min). Since the heating of the specimen by the punch continues and increases as the test proceeds, the temperature of the specimen was monitored throughout the whole test, not only in the heating phase before the punch movement, in order to achieve a fracture at the predefined temperature level. A set of each type of specimen used for the experimental plan is shown in Table 2: deformed sheets allow us to highlight the effect of temperature increase on the strain level.

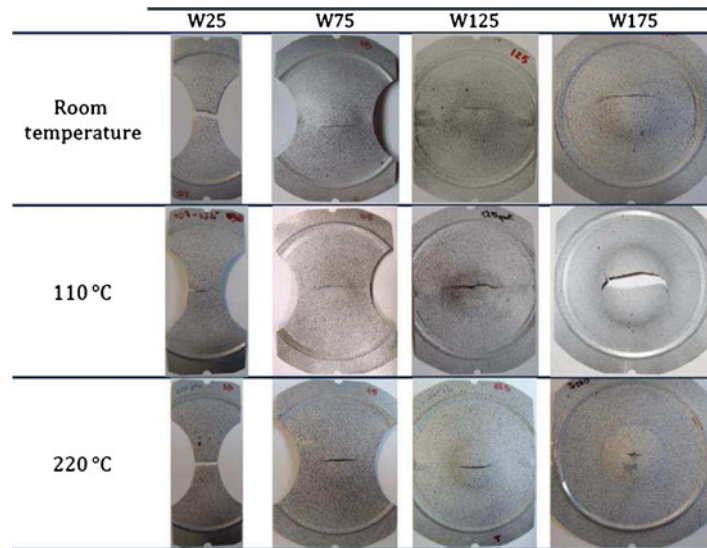


**Fig. 5** Flow stress curves of the AA6061 at different temperature and strain rate levels

The procedure detailed in the ISO Standard for evaluating FLCs was used in this work. This procedure is based on an analysis of the strain distribution along predefined cross sections. By removing the strain points in the necked area, the strain distribution just before the onset of necking is reconstructed in this region by curve fitting the remaining part of the strain distribution on both sides of the neck. The following steps were thus implemented to evaluate limit strains fitted by FLCs:

- Defining the relevant sections containing the neck (three sections intersecting the crack line, of a length of at least 20 mm on each side of the crack, with at least 10 points);
- Determining the neck region by an objective mathematical criterion (as shown in Fig. 6, the left inner limit (Bl) and the right inner limit (Br) defining the limits of the neck region, were evaluated using the second derivative criterion);
- Defining outer limits in order to obtain an optimal width of the fit window, that enables the best curve approximation relevant for both sides of the neck (the extension of the fit window is a function of the strain level reached in the points corresponding to the inner limits Br and Bl);
- Evaluating the best-fit inverse parabola ( $f_1(x)=1/(ax^2+bx+c)$ ) able to interpolate strain data in both left and right windows in order to determine the value in the apex (crack position) which is the desired limit for the major strain ( $\epsilon_1$ );
- determining the limit for the minor strain  $\epsilon_2$  indirectly through the best fit based on the true thickness strain (the thickness strain values are obtained by:  $\epsilon_3=-\epsilon_1-\epsilon_2$ ).

Additional points from the tensile tests were determined considering critical strain  $\epsilon_1 - \epsilon_2$  before the necking occurrence (the strain path deviation from linearity).

**Table 2** Specimens composing the experimental plan aimed at investigating the formability of AA6061-T6

Since the ISO standard allows for the use of “in-house” functions for the regression of  $\varepsilon_1$ - $\varepsilon_2$  data, left and right side points were fitted using two different equations, but setting the same intercept with the  $\varepsilon_1$  axis ( $FLD_0$ ). In particular, a second-order polynomial equation was used to fit data with  $\varepsilon_2 > 0$  while a linear equation was used to fit data with  $\varepsilon_2 < 0$ . This approach for fitting data allowed us to obtain FLCs that were characterised by a shape more similar to a Hill–Swift type [22] and was preferable to a single second order polynomial equation (used for example by Li and Ghosh [10] for fitting experimental data from biaxial forming tests) since it would have determined a trough position that did not correspond to a plane strain condition.

**Fig. 6** Example of results obtained applying the ISO standard procedure for the evaluation of limit strains

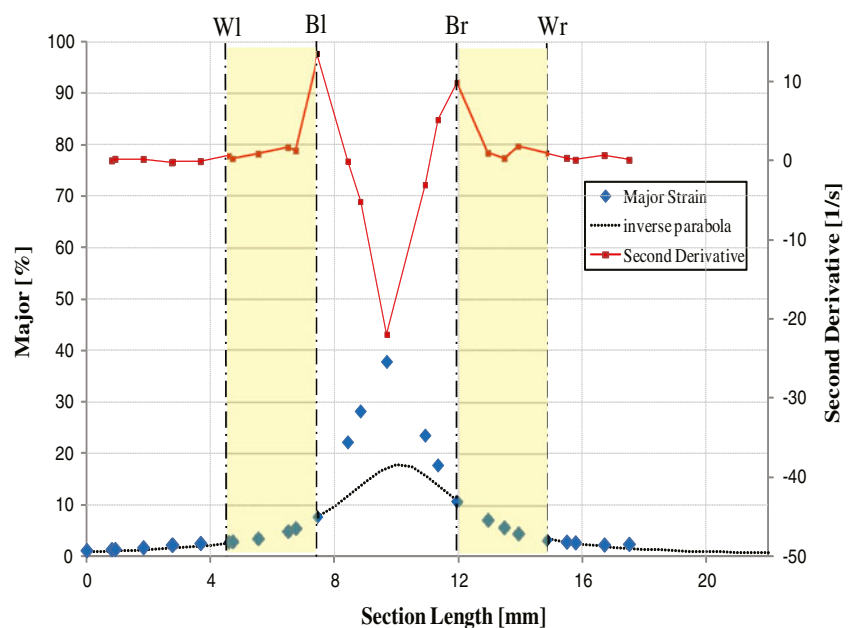


Figure 7 shows the FLCs at the three temperature levels evaluated using data from the four specimen geometries and from the tensile test specimen.

The FLC at RT shows good agreement with the experimental data in the work of Djvanroodi and Derogar [23]. In addition, the formability improvement of AA6061 at higher-than-room temperatures (almost entirely absent in literature) is coherent with the results presented by Li and Ghosh [10] in terms of amount of variation but substantially different in terms of strain value. In the abovementioned study, the authors simply determine a forming limit band which is the best fitting for experimental data points around a cracked area on rectangular cup parts. Even if the investigated alloy appears more

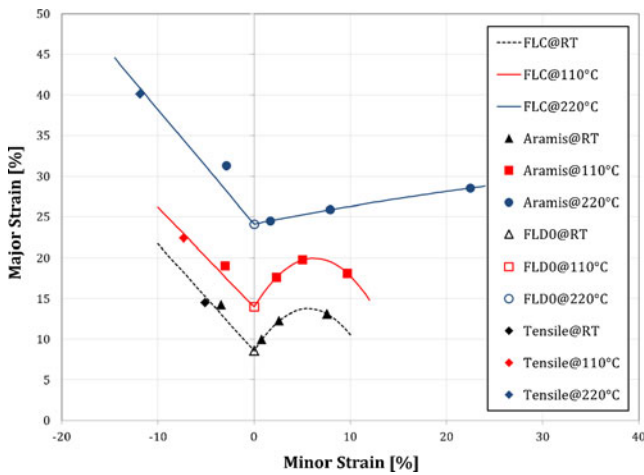


Fig. 7 Forming limit curves at different temperature levels

limited than other Al alloys, its improvement in terms of formability is worth noting, especially if the imposed (albeit somewhat limited) temperature increase is considered.

#### 4 Analysis of the channel profile using 2D models

With the aim of investigating the effect of channel geometrical parameters on the forming process, a low time-consuming 2D analysis was carried out. In fact, as shown by Fig. 8, the profiles of investigated BP types are almost identical.

##### 4.1 2D FE model description

Since simulations simply aimed to investigate the effect of geometrical features, the RT and the maximum forming pressure of 450 bar were assumed. The 2D plane strain model of the HF process was created using ABAQUS\Standard. The die was modelled as a rigid surface and the plane strain (PE) quadrilateral element typology was chosen for the mesh of the blank (4 elements along the thickness). Material behaviour was modelled using flow stress data at RT. For the yield surface, even if many other suitable functions exist for modelling Al alloys [22], the Von Mises yield function was adopted in this study. In fact, the adoption of more appropriate yield criteria able to model the “anomalous” behaviour of Al alloys [22] requires more complex tests, especially at elevated temperatures (equibiaxial tension state). Indeed, the adoption of the Von Mises yield behaviour was confirmed by other authors who simulated the Al alloy plastic behaviour to



Fig. 8 Profiles of the investigated BP types: a SER, b SP and c MSER

determine a relatively limited and acceptable deviation of results [24].

##### 4.2 Investigated parameters and conditions

The design of experiment technique was adopted to understand which geometrical parameters of the channel profile have the strongest effect on the forming process. According to literature [7, 17, 25] the most important design variables for the FC BP channels are the fuel channel width (**F**), the rib width or the land between two adjacent fuel channels (**S**), the channel depth (**h**) and the die upper radius (**R**). In addition, sheet thickness (**t**) can also be considered a design variable since it affects the channel section where both reagents and cooling water flow. In order to reduce the number of design variables, the channel depth was assumed as equal to the die radius ( $h=R$ ). Indeed, in the work of Peng et al. [17] (who take into account both formability and reaction performance), optimum dimension values for channel depth and transition radius are equal. In addition, the rib width was not considered in the present investigation since it appeared not to affect the forming process [17, 26].

Using a full factorial design (FFD), three different parameters were investigated simultaneously (by varying the levels of the factors rather than considering them one at a time) in order to evaluate interactions between them: the reagent channel width (**F**), the die upper radius (**R**) and the sheet thickness (**t**). The complete set of FE simulations is listed in Table 3.

Each combination of factor levels represents the conditions at which a response measurement was taken. In particular, for this analysis the following objective function was used as a response parameter:

Table 3 Summary of FE simulations according to the FFD

	<i>F</i> (mm)	<i>R</i> (mm)	<i>t</i> (mm)
	2.0	0.8	0.4
	1.0	0.4	0.5
	1.0	1.2	0.5
	3.0	0.4	0.5
	3.0	1.2	0.5
	0.5	0.8	0.7
	2.0	0.2	0.7
	2.0	1.4	0.7
	2.0	0.8	0.7
	3.5	0.8	0.7
	1.0	0.4	0.9
	1.0	1.2	0.9
	3.0	0.4	0.9
	3.0	1.2	0.9
	2.0	0.8	1.0

$$Obj = \ln\left(\frac{h_{eq}}{t_{eq}}\right) \quad (1)$$

with  $h_{eq}$  as the ratio between the height of the formed sheet and the depth of the die and  $t_{eq}$  as the ratio between the minimum thickness of the formed blank and the original thickness of the sheet. Both the parameters described above are taken as calculations performed at the end of the forming process, when the maximum pressure of 450 bar is reached.

### 4.3 Analysis of 2D FE results

A statistical approach was used to analyse data from the two-level FFD described above. In particular, the analysis of variance technique was used to evaluate the statistical significance of the factors. The regression model, interpolating data from simulations, was characterised by a coefficient of determination ( $R^2$ ) of 98.12 %, indicating its effectiveness in fitting the input data. Table 4 shows the coefficients of the regression model and their relative percentage weight, together with probability values ( $p$  values) of each effect (both linear and interaction).

The  $p$ -value of a factor represents the probability of committing an error when considering the mean value variation which is actually determined by the variation of the factor itself; consequently, the  $p$ -value was used to understand which factors actually influence the response parameter shown in Eq. 1. In particular, it may be noted that all the main effect terms are among those characterised by  $p$  values lower than the adopted confidence level ( $\alpha$ -level equal to 0.05). In addition, parameter  $F$  shows a non-linear effect and non-negligible interactions between the other two factors.

Simulation results are summarised in Fig. 9 using a Response Surface plot: the third parameter ( $R$  in the plotted surface) was fixed at an intermediate value (0.8 mm).

**Table 4** Weights of coefficients of the regression models for significant factors affecting the shape of BP channels and correspondent  $p$  values

Term	Coefficient	Weight (%)	$p$ value
Constant	0.814	20.54	0.024
$F$	-1.0566	26.66	0
$R$	-0.252	6.36	0.026
$t$	0.5928	14.96	0.001
$F*F$	0.3488	8.80	0.035
$R*R$	0.0729	1.84	0.575
$t*t$	0.2382	6.01	0.108
$F*R$	0.2677	6.76	0.045
$F*t$	-0.3029	7.64	0.03
$R*t$	0.0169	0.43	0.874

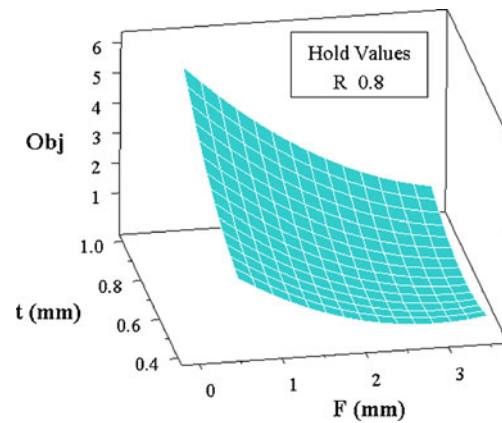


**Fig. 9** Response surface plotting of the values assumed by function  $Obj$  in the investigated range of parameters  $F$  and  $t$ , when fixing the value of  $R$  at 0.8 mm

It may be noted that, in order to minimise the value of the function  $Obj$ , thus ensuring a good performance of the Al alloy, the sheet thickness should be as low as possible. As a consequence, the value of  $t=0.5$  mm was chosen for subsequent analyses.

The contour plot in Fig. 10, showing the response parameter values as a function of the reagent channel width ( $F$ ) and the die upper radius ( $R$ ), highlights the fact that parameter  $F$  should be as large as possible in order to minimise the objective function. In particular, if choosing a value larger than 2.5 mm, independently of the value of  $R$ , the value of the function  $Obj$  lies in the region characterised by the lowest values. An optimal depth is thus given, which is reached by the formed sheet accompanied by a minimal thickness reduction. The channel profile characterised by  $F=3$  mm and by the relatively high value of  $R$  (1.2 mm) was thus chosen for the 3D numerical simulations outlined in the following section.

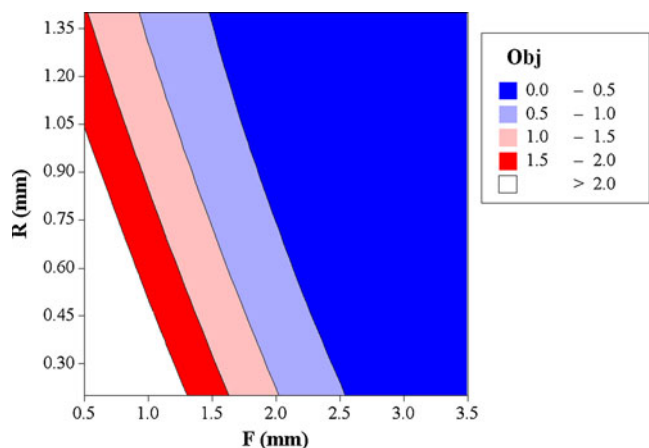


**Fig. 10** Contour plot of the function  $Obj$  in the investigated range of parameters  $F$  and  $R$ , when fixing the value of  $t$  at 0.5 mm



Kumar and Reddy [25] suggested in their study that, in order to maximise fuel consumption, the optimum channel depth should be 1.5 mm, which is in a good accordance with the one adopted in this work. Furthermore, using the model proposed in the abovementioned work, the value of  $F$  determined in the present analysis would determine not a maximum hydrogen consumption, but of nearly 80 %. The outcomes of this study also proved to be compatible with the results of Peng et al. [17]: indeed, their results showed that in order to maximise formability (in terms of risk of fracture due to material thinning), the die upper radius should be set at values nearing 1.5 mm.

### 5 Analysis of BP HF by 3D models

The analysis of the WHF process to manufacture the three different BP types was carried out using 3D models. Studies focused on both the effect of the die shape (changing according to the BP geometries) and the effect of the process parameters (pressure and temperature).

#### 5.1 3D FE model description

Different BP geometries and WHF process parameters were investigated using the commercial FE code ABAQUS/Explicit (v. 6.10). Die geometries were modelled as rigid bodies, while the sheet was modelled as a deformable part. The friction coefficient between the sheet and the tools surfaces was set at 0.05; such a low value of the friction coefficient appears to be reasonable due to the presence of the oil between the blank and both the blankholder and the die, but needs to be verified at higher-than-room temperatures since the viscosity of mineral oil based lubricants strongly reduce at elevated temperature [27]. As in the 2D simulations, the Von Mises yield function was used. Finally, a linear pressure profile was used and the hardening of the adopted Al alloy, according to  $T$  and  $SR$ , was modelled using the experimental data referred to in Section 3.

#### 5.2 Analysis of 3D FE results

Numerical simulations were carried out at the same temperature levels investigated in the experimental activity: RT, 110 and 220 °C. Two different pressure levels were set, according to the working temperature: 350 bar for the WHF process and 700 bar for the HF process (at RT). The difference in pressure levels was due to limitations in the experimental apparatus which is to be used for future tests. It consists of: (1) a 500-kN electro-hydraulic press machine equipped with a heated die able to reach a maximum temperature of 350 °C and (2) an oil pressurising unit able to work up to 350bar when using heated oil (up to 750 bar at RT).

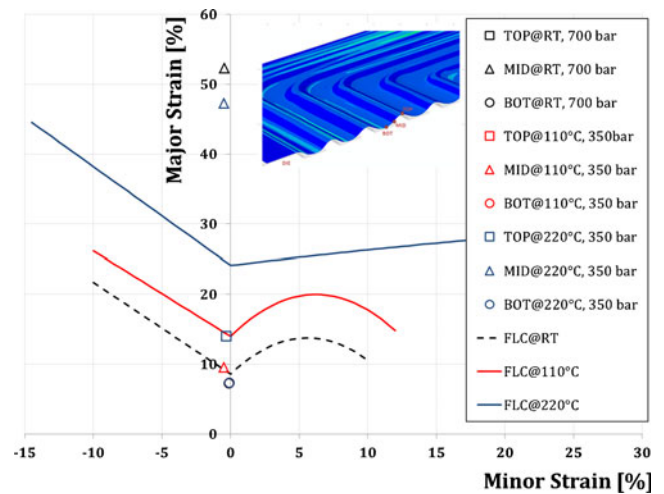


Fig. 11 Strain condition of various points along the profile of the BP type SP at different pressure levels and temperatures

The experimental Forming Limit Diagram of the investigated Al alloy was used to analyse the results of FE simulations. In particular, the occurrence of critical strain conditions was evaluated by comparing the strain pairs of critical points with the FLC. The region of the channel profile to be investigated was chosen by comparing the evolution of major and minor strains of three points: as shown in the scheme of Fig. 11, these points are located in the regions at the bottom (labelled BOT), top (labelled TOP) and side (labelled MID) of the channel. The BP geometry SP was adopted for this analysis.

In Fig. 11, the strain conditions (major and minor strain pairs) of each point at all temperature levels and at maximum pressure are plotted on the FLD of the Al alloy under

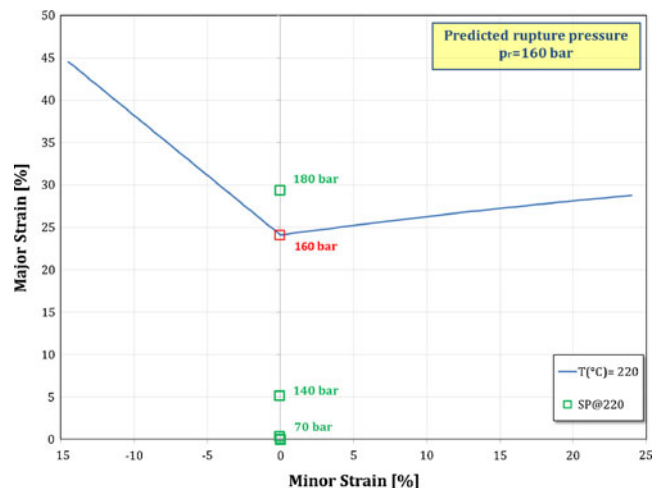


Fig. 12 Numerical evaluation of the maximum pressure level when using the SP die geometry and setting the temperature at 220 °C

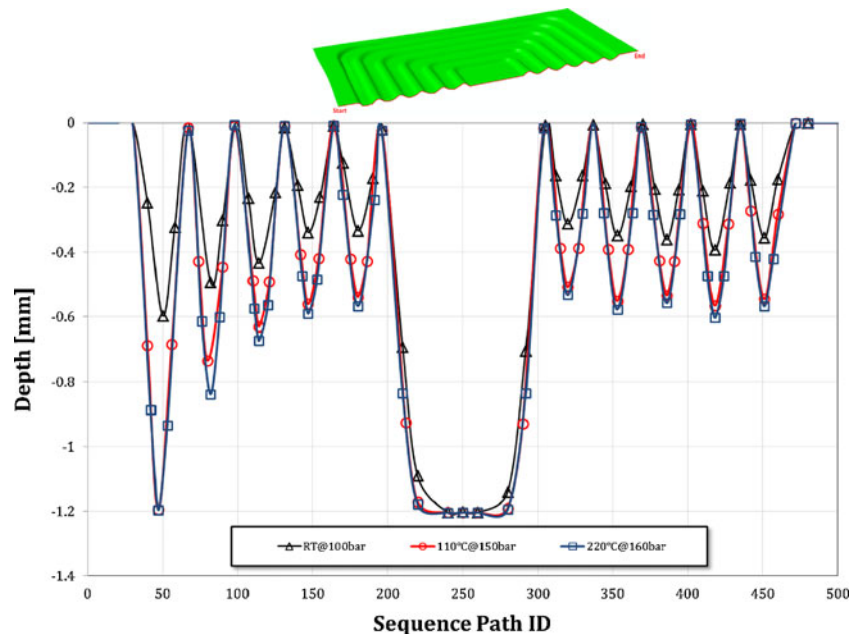
**Table 5** Summary of results by simulations using the three BP types and setting different pressure and temperature levels

Simulation details		PEEQ Map	Simulation details		PEEQ Map
Geometry	SP		Geometry	SER	
T (°C)	RT		T (°C)	220	
Max p (bar)	100		Max p (bar)	70	
Max PEEQ	23%		Max PEEQ	24%	
Geometry	SP		Geometry	MSER	
T (°C)	110		T (°C)	RT	
Max p (bar)	150		Max p (bar)	30	
Max PEEQ	23%		Max PEEQ	20%	
Geometry	SP		Geometry	MSER	
T (°C)	220		T (°C)	110	
Max p (bar)	160		Max p (bar)	50	
Max PEEQ	30%		Max PEEQ	25%	
Geometry	SER		Geometry	MSER	
T (°C)	RT		T (°C)	220	
Max p (bar)	30		Max p (bar)	80	
Max PEEQ	8%		Max PEEQ	28%	
Geometry	SER				
T (°C)	110				
Max p (bar)	40				
Max PEEQ	19%				

study. The MID points along the profile of the considered BP type are critical, since they are unsupported for a longer time during the forming process. It was thus used for subsequent analyses. The maximum pressure level was evaluated by comparing the strain path (major–minor strain

evolution during the process) of the most critical region in the MID position with the FLC corresponding to the adopted working temperature (as shown in Fig. 12 for the test carried out, setting the temperature at 220 °C and adopting the SP die geometry).

**Fig. 13** Channel profiles of the SP geometry obtained at different temperature levels



Results from all simulations adopting the BP geometries described above are summarised in Table 5 in terms of strain maps, maximum plastic equivalent strain (PEEQ) and maximum pressure level.

The first point to note from the comparisons shown in Table 5 is that BP geometry has a significant effect on the process, above all in terms of limit pressure. In fact, it is evident that the BP geometry SP presents the highest limit pressure values (after which rupture is expected) at all temperature levels. On the contrary, the BP geometry SER seems to be the most critical, allowing the lowest pressure levels to be used when working in warm conditions (at 110 or 220 °C). It is also interesting to note that the highest pressure levels are always reached when working in warm conditions. Indeed, these working conditions determine a formability increase accompanied by a limited material strength decrease and, as a consequence, a limit pressure value higher than the pressure at RT for all geometries.

As regards strain distributions, it can be noted that the PEEQ maps for simulations using the BP geometry SP do not present dangerous strain localisations, as is evident in the case of the BP geometries SER and MSER. In particular, the three geometries exhibit a similar (increasing) trend for the PEEQ according to temperature. However, irrespective of the comparable maximum PEEQ values, in the BP geometries SER and MSER these values are localised in small areas (the critical zones shown by white circles) where the strain increases rapidly, leading to rupture at low working pressure.

Results in Table 5 highlight the key role played in the process by parameter  $T$ , which determine an increase of both strain and limit pressure levels. Since the maximum PEEQ strain level is a local piece of data, it is interesting to analyse the channel profiles on the whole BP after the forming process. The channel profiles acquired when the limit pressure values are applied are plotted in Fig. 13, with a clear focus on the BP geometry SP which is the one characterised by the largest PEEQ when increasing the temperature.

The profiles in warm conditions are confirmed as the closest to the die cavity shape and the improvement is clear. However, what is more important is that the channel profiles at 220 °C show relatively small differences when compared with the profiles at 110 °C.

This result confirms the progressive reduction of benefits deriving from the temperature increase. This is also highlighted in the work of Mahabunphachai and Koc [19] who performed HF experiments on the same alloy and noticed that at 200 °C, a forming pressure increase from 10 to 20bar determined a die filling increase from 60 to 83 %, while at 300 °C, the same forming pressure determined almost no die filling improvement.

It can be thus concluded that the adoption of a temperature level higher than 110 °C appears to be inconvenient if considering the improvement in terms of die cavity filling

combined with the difficulty of reaching a temperature of 220 °C (by both oil and die).

## 6 Conclusions

Different types of BP geometries have been proposed in this research study; SER, SP and MSER. In order to manufacture these geometries using HF and thin, light sheets (an AA6061 Al alloy was assumed), the BPs geometries were designed considering two constraints: (1) channels on both sides of the BP have to be created in a single forming step; (2) the layout of channels must allow for the separation of both reagents and coolant. All geometries represent viable solutions for industrial applications, since they can determine strong thickness reduction of the component, thus leading to an increase in the specific energy produced by the PEMFC and/or to a weight reduction of the cell. For example, the proposed BP types can be implemented in PEMFC stacks to be used in the power supply of compact electric cars since they have an active area which is greater than the minimum required for this application.

The preliminary experimental feature of the AA6061 alloy highlights the fact that temperature affects both its strength and formability.

Numerical analysis, using both 2D and 3D FE models, allowed for:

- A definition of the optimal shape for the BP channels in the range of the explored parameters (the die upper radius,  $R=0.5$  mm, the reagent channel width,  $F=3$  mm).
- An evaluation of the effect of BP geometry on the forming process (the geometry labelled SP was characterised by uniform strain distribution and enabled the adoption of the highest forming pressure value at any working temperature).
- An evaluation of the key role played by parameter temperature on the HF of a BP, in particular that with SP geometry the channel profile at 220 °C proved to be the nearest to the die cavity profile, even if the most moderate temperature increase (up to 110 °C) determines the most convenient process improvement.

Future developments of this research will aim to: (1) investigate the effect of anisotropy on material properties, (2) evaluate the effect of modelling the anisotropy in the FE simulation of the warm HF process using a suitable yield criterion, (3) perform experimental tests using the combined Warm HF/Superplastic Forming press machine described in Subsection 5.2 and (4) to validate numerical results and assumptions.

**Acknowledgements** The authors would like to express their gratitude to the Apulia Region for their support in this research activity through the establishment of the TRASFORMA laboratory network

(cod. 28). In addition, contributions by mechanical engineers M. Montemurro and V. Piglionico were greatly appreciated.

## References

- EG&G Technical Services, Inc. (2004) Fuel cell handbook (seventh edn). U.S. Department of Energy, Morgantown
- Carton JG, Olabi AG (2010) Design of experiment study of the parameters that affect performance of three flow plate configurations of a proton exchange membrane fuel cell. *Energy* 35:2796–2806
- Woodman AS, Anderson EB, Jayne KD, Kimble MC (1999) Development of corrosion-resistant coatings for fuel cell bipolar plates. Physical Sciences Inc., Andover, pp 1–9
- Cunningham B (2007) The Development of compression moldable polymer composite bipolar plates for fuel cells. Ph.D. dissertation, Faculty of Virginia Polytechnic Institute and State University
- Jeswiet J, Geiger M, Engel U, Kleiner M, Schikorra M, Dufloy J, Neugebauer R, Bariani P, Bruschi S (2008) Metal forming progress since 2000. *CIRP J Manuf Sci Technol* 1:2–17
- Dihrab SS, Sopian K, Alghoul MA, Sulaiman MY (2009) Review of the membrane and bipolar plates material for conventional and unitized regenerative fuel cells. *Renew Sustain Energy Rev* 13:1663–1668
- Turan C, Cora ÖN, Koç M (2011) Effect of manufacturing processes on contact resistance characteristics of metallic bipolar plates in PEM fuel cells. *Int J Hydrog Energy* 36:12370–12380
- Peker MF, Cora ÖN, Koç M (2011) Investigation on the variation of corrosion and contact resistance characteristics of metallic bipolar plates manufacturer under long-run conditions. *Int J Hydrog Energy* 36:15427–15436
- Barranco F, Barreras A, Lozano MM (2011) Influence of Cr–N coating thickness on the corrosion resistance behaviour of aluminium-based bipolar plates. *J Power Sources* 196:4283–4289
- Li D, Ghosh AK (2004) Biaxial warm forming behavior of aluminium sheet alloys. *J Mater Process Technol* 145(3):281–293
- Li D, Ghosh A (2003) Tensile deformation behavior of aluminum alloys at warm forming temperatures. *Mater Sci Eng A* 352(1–2):279–286
- Naka T, Torikai G, Hino R, Yoshida F (2001) The effects of temperature and forming speed on the forming limit diagram for type 5083 aluminum–magnesium alloy sheet. *J Mater Process Technol* 113:648–653
- Masuda T, Kobayashi T, Wang L, Toda H (2003) Effects of strain rate on deformation behavior of A6061-T6 aluminum alloy. *Mater Sci Forum* 426–432:285–290
- Zhang SH, Wang ZR, Xu Y, Wang ZT, Zhou LX (2004) Recent developments in sheet hydro-forming technology. *J Mater Process Technol* 151(1–3):237–241
- Palumbo G, Pinto S, Tricarico L (2004) Numerical/experimental analysis of the sheet hydro forming process using cylindrical, square and compound shaped cavities. *J Mater Process Technol* 155–156(1–3):1435–1442
- Mahabunphachai S, Koc M (2007) Feasibility investigations on a novel micro-manufacturing process for fabrication of fuel cell bipolar plates: Internal pressure-assisted embossing of micro-channels with in-die mechanical bonding. *J Power Sources* 172(2):725–733
- Peng L, Lai X, Liu D, Hu P, Ni J (2008) Flow channel shape optimum design for hydroformed metal bipolar plate in PEM fuel cell. *J Power Sources* 178:223–230
- Lang LH, Wang ZR, Kang DC, Yuan SJ, Zhang SH, Danckert J, Nielsen KB (2004) Hydroforming highlights: sheet hydroforming and tube hydroforming. *J Mater Process Technol* 151(1–3):165–177
- Mahabunphachai S, Koc M (2010) Investigations on forming of aluminum 5052 and 6061 sheet alloys at warm temperatures. *Mater Des* 31:2422–2434
- Johansson M, Hornqvist M, Karlsson B (2006) Influence of temperature and strain rate on the plastic deformation of two commercial high strength Al alloys. *Mater Sci Forum* 519–521:841–846
- International Standard ISO 12004-2 Metallic material sheet and strip—determination of forming-limit curves—part2: determination of forming limit curves in the laboratory. First edition 15-10-2008
- Bunge HJ, Pöhlandt K, Tekkaya AE, Banabic D (2000) Formability of metallic materials. Springer, Berlin
- Djvanroodi D (2010) Experimental and numerical evaluation of forming limit diagram for Ti6Al4V titanium and AA6061-T6 aluminium alloys sheets. *Mater Des* 31:4866–4875
- Gedikli H, Cora ON, Koç M (2010) Comparative investigations on numerical modeling for warm hydroforming of AA5754-O aluminum sheet alloy. *Mater Des* 32:2650–2662
- Kumar A, Reddy RG (2003) Effect of channel dimensions and shape in the flow-field distributor on the performance of polymer electrolyte membrane fuel cells. *J Power Sources* 113:11–18
- Palumbo G, Montemurro M (2011) Warm hydroforming of an aluminium bipolar plate for proton exchange membrane fuel cells. In: 10th International Conference on Technology of Plasticity-ICTP, Aachen, Germany, pp. 449–454. ISBN 978-3-514-00784-0
- Groche P, Huber R, Dörr J, Schmoedel D (2002) Hydromechanical deep-drawing of aluminium-alloys at elevated temperatures. *CIRP Ann Manuf Technol* 51(1):215–218